nature materials

LETTERS

PUBLISHED ONLINE: 25 OCTOBER 2009 | DOI: 10.1038/NMAT2561

Experimental demonstration of an acoustic magnifying hyperlens

Jensen Li[1]*, Lee Fok[1]*, Xiaobo Yin[1,2], Guy Bartal[1] and Xiang Zhang[1,2]†

Acoustic metamaterials can manipulate sound waves in surprising ways, which include collimation, focusing, cloaking, sonic screening and extraordinary transmission[1–14]. Recent theories suggested that imaging below the diffraction limit using passive elements can be realized by acoustic superlenses or magnifying hyperlenses[15,16]. These could markedly enhance the capabilities in underwater sonar sensing, medical ultrasound imaging and non-destructive materials testing. However, these proposed approaches suffer narrow working frequency bands and significant resonance-induced loss, which hinders them from successful experimental realization. Here, we report the experimental demonstration of an acoustic hyperlens that magnifies subwavelength objects by gradually converting evanescent components into propagating waves. The fabricated acoustic hyperlens relies on straightforward cutoff-free propagation and achieves deep-subwavelength resolution with low loss over a broad frequency bandwidth.

Magnifying optical hyperlenses[17,18] have shown the ability to overcome the diffraction limit in electromagnetic waves, imaging objects with a resolution significantly smaller than half the wavelength. By using carefully engineered dispersion surfaces obtained using metamaterials, these hyperlenses not only carry the subwavelength information contained in evanescent waves across the lens, but also magnify it, thereby converting it to propagating waves such that the information travels to the far field outside the lens. The first demonstrated optical hyperlenses used two-dimensional (2D) metamaterials consisting of deep-subwavelength layers of metals and dielectrics alternating in the radial directions, to constitute a largely negative effective permittivity along the propagation (radial) direction, and at the same time small effective permittivity at the transverse (angular) direction[17,18]. For such anisotropic material properties, the 2D dispersion curves are hyperbolic and nearly flat over a wide range of angular wavevectors, indicating that high-angular-momentum optical modes are supported as propagating waves, allowing the subwavelength information to propagate in the material. The successful demonstration has motivated the search for new forms of magnifying lens with subwavelength resolution. These include plasmonic or transverse electromagnetic modes propagating among tapered wires[19–21], sampling a subwavelength image pixel-by-pixel to create the magnified image at the lens exit.

As the diffraction limit is intrinsic to all kinds of wave phenomenon, conventional acoustic imaging is also limited by the wavelength of the sound wave. Therefore, an acoustic superlens or hyperlens, if realized, will readily benefit applications such as non-destructive testing and medical imaging. Recent studies have shown that acoustic focusing can be achieved by using phononic crystal slabs[22–27] and acoustic metamaterials[28]. To the best of our knowledge, there has been no experimental demonstration of deep-subwavelength imaging in acoustics using either phononic crystals or metamaterials. A recent theory of acoustic metamaterial hyperlenses has effectively used alternating layers of positive and negative dynamic density, using locally resonant acoustic elements to achieve the negative density and flat dispersion curve[16]. However, the negative dynamic density[1,29] can occur only at a narrow band of frequencies when these elements oscillate resonantly, introducing excessive loss that is associated with such a sharp resonance. This limits the maximum propagation distance and subsequently restricts the practically achievable magnification.

Here, we propose and demonstrate a new type of acoustic hyperlens, using a non-resonant radially symmetric layered structure. We show experimentally broadband low-loss imaging with large magnification, where the evanescent-wave components associated with the deep-subwavelength features are gradually converted into propagating waves that travel to the far field.

Our acoustic hyperlens consists of 36 brass fins (Fig. 1), which are 3 mm tall and extend from 2.7 to 21.8 cm from the centre of a half-cylinder. Each fin occupies 2.5° in the angular direction, with 2.5° left as space between adjacent fins. The fabrication was done by a two-axis computer-numerical-controlled vertical mill. The hyperlens was milled off from a 0.5-inch-thick brass plate, resulting in the brass fins on the remaining substrate of 9.7 mm in thickness, more than sufficient to prevent wave leakage. A 0.25-inch-thick aluminium plate covers the top of the fins to confine the sound propagation region to two dimensions. Holes were drilled in the cover plate to measure the sound at varying distances, and the top plate rotates to allow pressure mapping in the angular direction. Experimental details are provided in the Supplementary Methods. Two in-phase 1-cm-diameter sound sources transmitting at 4.2–7.0 kHz with separation of 1.2 cm (corresponding to $\lambda/6.8$–$\lambda/4.1$) are placed in front of the inner edge of the lens while the pressure amplitude and phase were measured from 0.4–9.9 cm away from the outer edge of the lens. The distance of 9.9 cm corresponds to 1.2λ at 4.2 kHz and 2λ at 7.0 kHz.

Owing to the large ratio between the outer and the inner radii, the hyperlens compresses a significant portion of the evanescent components into the band of propagating waves such that the image is magnified eight times, the subwavelength sources themselves radiating at the lens outer edge as if they are larger than the diffraction limit for the frequency range of interest. Figure 2a shows the propagation of an object consisting of the two sound sources transmitting at 6.6 kHz and separated by 0.23λ at the input plane. The separation is converted to 1.85λ and the sources are magnified to be larger than one wavelength at the hyperlens exit such that it can also be observed in the far field as two distinct beams. A similar magnification is observed for a three-source system in which the

[1]NSF Nano-scale Science and Engineering Center (NSEC), 3112 Etcheverry Hall, University of California, Berkeley, California 94720, USA, [2]Material Sciences Division, Lawrence Berkeley National Laboratory, Berkeley, California 94720, USA. *These authors contributed equally to this work.
†e-mail: xiang@berkeley.edu.

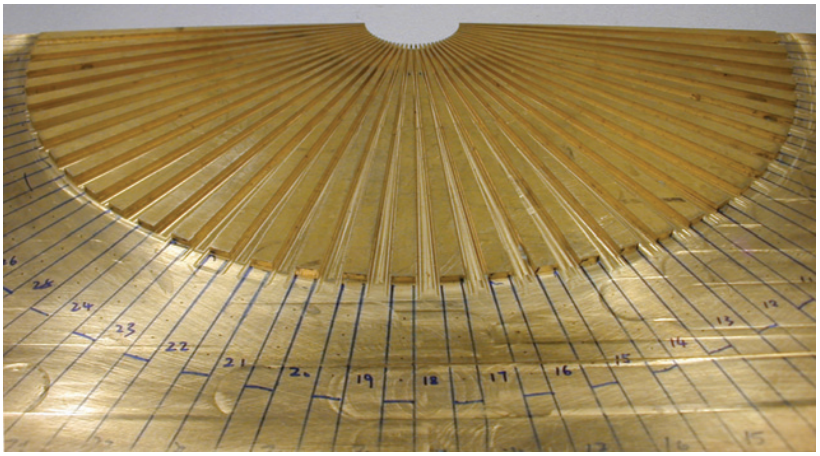

Figure 1 | Acoustic hyperlens. The lens is made of 36 brass fins (running radially from a radius of 2.7 to 21.8 cm) in air embedded on a brass substrate, spanning 180° in the angular direction. The cover sheet has been removed to expose the microstructure for this view.

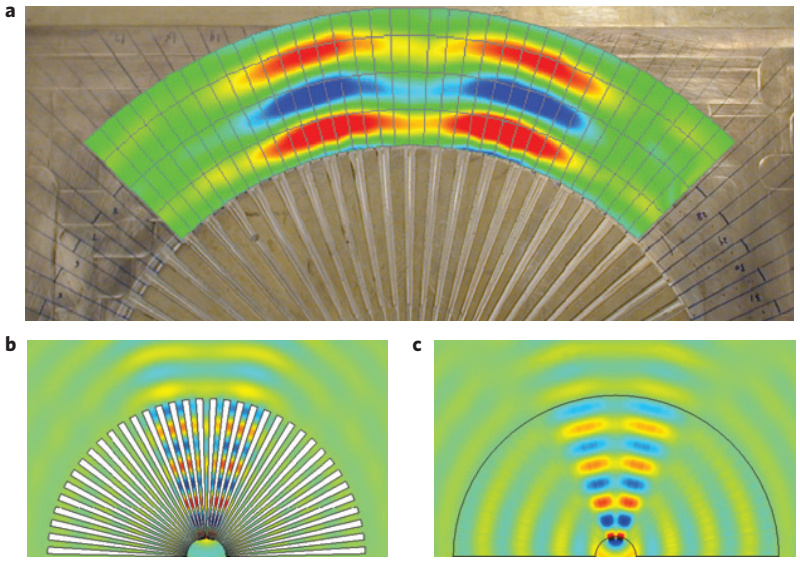

Figure 2 | Experimental magnifying imaging of a dual-source sub-diffraction-limited object at 6.6 kHz. a, Experimental pressure measurements in the propagation region. The pressure is measured at various points ranging from 0.4 to 9.9 cm away from the lens. **b**, 3D simulation of the pressure field using the microstructure including elastic fins. **c**, 2D simulation using the effective medium description of the lens. The experimental and numerical results show the propagating nature of the magnified subwavelength object. The red/blue colour indicates high/low instantaneous pressure values. Simulation details are provided in the Supplementary Methods.

sources are asymmetrically positioned in the Supplementary Data and Fig. S1. The results obtained from the ×8 magnifying hyperlens stand in sharp contrast to the signal measured in the absence of the hyperlens at the outer edge of the lens, where the two peaks cannot be resolved owing to the diffraction limit (Fig. 3a). Figure 2b shows the three-dimensional (3D) simulations obtained using COMSOL Multiphysics 3.4 (consisting of the elastic fins, substrate, top plate and air) with the pressure field plotted at 1.5 mm from the substrate, which agrees well with the experimental results. We have also carried out the 2D simulation for the same configuration using properties from the effective medium description, shown in Fig. 2c. The good agreement between the experiment, the 3D simulation with microscopic structures and the 2D simulation with effective medium parameters results from the subwavelength periodicity of the hyperlens, which even at the outer radius (eight times larger than at the inner radius) is still around one third of the wavelength, making the effective medium approximation valid.

To further confirm that the lens has successfully converted evanescent components into propagating components, we measured the amplitude and phase along one of the two beams exiting the hyperlens (Fig. 3b). A wave composed primarily of propagating components should decay approximately as $1/r^{1/2}$ owing to geometric spreading and have a phase speed close to that of air, whereas one composed primarily of evanescent waves should decay exponentially and have nearly constant phase. Our measurements show a slow decay in the amplitude and linear phase progress outside the lens, demonstrating the conversion of evanescent components into propagating waves. Moreover, as our design does not involve any local resonance, it can operate over a broadband of frequencies without significant loss. Figure 4 shows the measured broadband response of the hyperlens, with the subwavelength resolution ($\lambda/6.8$–$\lambda/4.1$) for frequencies varying from 4.2 to 7.0 kHz.

The term 'hyperlens' was originally coined for an ideal indefinite medium with negative permittivity along one direction, resulting in hyperbolic equi-frequency contours[30]. Although this should support unlimited resolution, in reality, the performance of a hyperlens is limited by the material's properties, such as the intrinsic loss and periodicity. Optical hyperlenses require extreme values

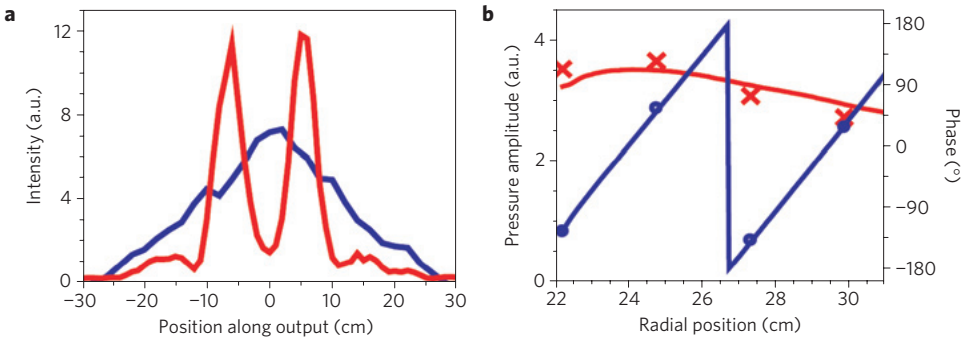

Figure 3 | Hyperlens imaging at 6.6 kHz. a, The magnified image at the outer edge of the lens (red line) clearly maintains the $\lambda/4.3$ resolution, in contrast to the control experiment (blue line), showing a single peak, measured at the same position under similar conditions but in the absence of the hyperlens. **b**, Radial dependence of the pressure field (amplitude in red and phase in blue) along the centre of one of the two beams. The crosses and open circles show the measured data points and the solid lines are the simulation results. The phase advance and the slow amplitude decay clearly demonstrate that the originally evanescent sound wave is converted to a propagating one, while maintaining the subwavelength features of the object.

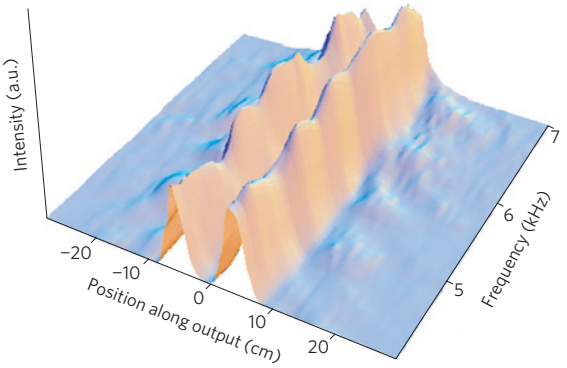

Figure 4 | The broadband performance of the acoustic hyperlens. Experimental measurement of the pressure intensity against position and frequency, measured at the outer edge of the lens. The frequency ranges from 4.2–7 kHz, corresponding to a $\lambda/6.8$–$\lambda/4.1$ resolution. The intensity profile at each frequency is scaled so the two peaks can be clearly resolved throughout the frequency range.

for the constituents' properties, which in turn require layers with negative permittivity, imposing intrinsic losses associated with plasmonic or local resonance. Acoustic hyperlenses, on the other hand, are very different; here, extreme values of effective density can be obtained using non-resonant materials. Namely, the propagation and magnification ratio can be unlimited. As no negative density is required, the equi-frequency contours of such a lens are elliptic and described by equation (1).

$$\frac{k_r^2}{\rho_r}+\frac{k_\theta^2}{\rho_\theta}=\frac{\omega^2}{B} \tag{1}$$

In equation (1), B is the effective bulk modulus, k_r and k_θ are the wavevector components along the radial and angular directions, respectively, and ρ_r and ρ_θ are the effective densities along the radial and angular directions, both positive; ω is the frequency of the acoustic wave. The general derivation of this equation has been done previously[31]. This equation differs from the electromagnetic form owing to the longitudinal nature of acoustic waves, as opposed to transverse in electromagnetism. An angular effective density much larger than the radial one results in a nearly flat equi-frequency contour, indicating that this metamaterial allows propagation of modes with high tangential momentum that carry the sub-diffractional spatial information of the object.

In our non-resonant hyperlens design, the extreme anisotropy is achieved by perforating a solid with a cross-section that linearly expands in the radial direction. The subwavelength spacing of the perforations throughout the hyperlens allows the use of effective medium properties for the bulk modulus B, and the densities ρ_r and ρ_θ, which are assigned as follows:

$$\frac{1}{\rho_r}=\frac{f}{\rho_1}+\frac{1-f}{\rho_2} \tag{2}$$

$$\rho_\theta=f\rho_1+(1-f)\rho_2 \tag{3}$$

$$\frac{1}{B}=\frac{f}{B_1}+\frac{1-f}{B_2} \tag{4}$$

In these equations, f is the volume filling ratio of the fins, ρ_1 and B_1 are the fin material density and bulk modulus, respectively, and ρ_2 and B_2 are the filling fluid density and bulk modulus, respectively. These equations can be obtained using an analogy between transverse magnetic electromagnetic waves and acoustic waves found in the Supplementary Discussion. The ability of the fins to support shear waves has been neglected in these equations owing to the large contrast in density in the design materials. It has previously been shown that in solid–fluid systems with a large density contrast, the influence of these modes is negligible[32]. Details on the fin vibrations in our structure can be found in the Supplementary Data and Fig. S2.

To achieve the strong anisotropy required for the flat dispersion, the constituent materials must also preserve a large ratio of material densities. We therefore have chosen brass to be the fin material, as it has a density about 7,000 times that of air. Such an extreme ratio between the constituents' properties cannot be achieved for optical frequencies without involving a resonance. The maximum permittivity contrast available in dielectrics is about ten at these frequencies, and any larger contrast will require the use of a resonance, for example, by incorporating metals in the structure. We calculate the equi-frequency contour for the brass–air composite with a filling ratio of 0.5 using both the transfer matrix method (blue line; see Supplementary Discussion) and the effective medium approximation (green line; see equations (2)–(4)), shown in Fig. 5. The effective medium description approximates well the actual dispersion even up to a high tangential momentum, indicating that the hyperlens can indeed be treated as an effective medium metamaterial. For comparison, we plot the dispersion curve of a hyperlens with a negative effective density in the angular direction, but with similar magnitude. As long as the dispersion is flat for a large range of wavevectors, both hyperbolic and elliptical dispersion work equivalently well. By using elliptical instead of hyperbolic dispersion, we avoid the use of resonating elements in constructing the metamaterial. Within the effective medium description, the angular momentum

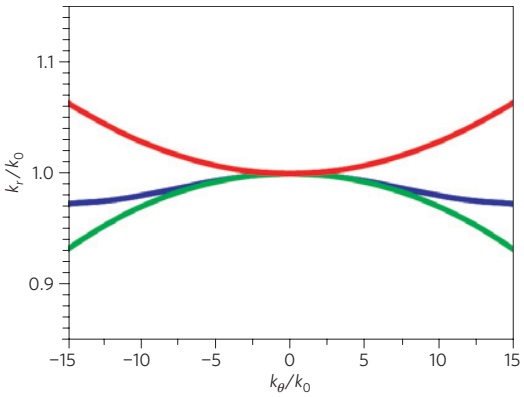

Figure 5 | Hyperlens equi-frequency contour. The hyperlens equi-frequency contour calculated using the transfer matrix method on the actual microstructure is shown in blue. The green line shows the elliptical equi-frequency contour using the effective medium approximation in place of stacking alternating layers of air and brass. These agree well over a large range of angular wavevectors, supporting the use of the effective medium theory. The red curve shows the hyperbolic equi-frequency contour of a hyperlens with material properties the same magnitude as the green effective medium curve, but negative effective density in the angular direction. The large flat region in all of the equi-frequency contours demonstrated that both hyperbolic and elliptical dispersions can be used to construct a hyperlens. For the green and blue curves, the filling ratio $f = 0.5$, the lattice constant is 2 mm and the working frequency is 6.6 kHz.

of the sound wave propagating along the radial direction is conserved owing to the cylindrical symmetry. Hence, the linear tangential momentum is compressed during the outward propagation, thereby magnifying the subwavelength details of the object[17].

The absence of local acoustic resonances allows in principle very large propagation distances and hence very large magnification ratios, as long as the microstructure periodicity remains in the effective medium approximation. This is in contrast to optical hyperlenses, where the magnification is limited by the loss associated with plasmonic resonance. Although the increase of the period length may impose a limit on the magnification ratio, this limitation can be overcome by cascading extra hyperlens layers, consisting of a larger number of fins with the same filling ratio of brass, maintaining the subwavelength periodicity along the lens (see Supplementary Fig. S3).

As the velocity fields of the acoustic waves are polarized only along the propagation directions, a 3D hyperlens can be constructed by perforating a hemisphere solid with tapered holes in the radial direction. Such a configuration is not subject to the complications arising from the polarization-dependent plasmonic confinement in optical hyperlenses, and hence allows the magnification of subwavelength features in all directions. Such a high-magnification-ratio acoustic hyperlens, with the ability to break the diffraction limit, can find important applications in high-resolution ultrasonic medical imaging and underwater sonar.

Received 13 July 2009; accepted 23 September 2009; published online 25 October 2009

References

1. Liu, Z. *et al.* Locally resonant sonic materials. *Science* **289,** 1734–1736 (2001).
2. Fang, N. *et al.* Ultrasonic metamaterials with negative modulus. *Nature Mater.* **5,** 452–456 (2006).
3. Christensen, J., Fernandez-Dominguez, A. I., de Leon-Perez, F., Martin-Moreno, L. & Garcia-Vidal, F. J. Collimation of sound assisted by acoustic surface waves. *Nature Phys.* **3,** 851–852 (2007).
4. Christensen, J., Huidobro, P. A., Martin-Moreno, L. & Garcia-Vidal, F. J. Confining and slowing airborne sound with a corrugated metawire. *Appl. Phys. Lett.* **93,** 083502 (2008).
5. de Rosny, J. & Fink, M. Overcoming the diffraction limit in wave physics using a time-reversal mirror and a novel acoustic sink. *Phys. Rev. Lett.* **89,** 124301 (2002).
6. Greenleaf, A., Kurylev, Y., Lassas, M. & Uhlmann, G. Full-wave invisibility of active devices at all frequencies. *Commun. Math. Phys.* **275,** 749–789 (2007).
7. Milton, G. W., Briane, M. & Willis, J. R. On cloaking for elasticity and physical equations with a transformation invariant form. *New. J. Phys.* **8,** 248 (2006).
8. Chen, H. & Chan, C. T. Acoustic cloaking in three dimensions using acoustic metamaterials. *Appl. Phys. Lett.* **91,** 183518 (2007).
9. Cummer, S. A. *et al.* Scattering theory derivation of a 3D acoustic cloaking shell. *Phys. Rev. Lett.* **100,** 024301 (2008).
10. Farhat, M. *et al.* A homogenization route towards square cylindrical acoustic cloaks. *New J. Phys.* **10,** 115030 (2008).
11. Torrent, D. & Sánchez-Dehesa, J. Acoustic cloaking in two dimensions: A feasible approach. *New J. Phys.* **10,** 063015 (2008).
12. Norris, A. N. Acoustic metafluids. *J. Acoust. Soc. Am.* **125,** 839–849 (2009).
13. Estrada, H. *et al.* Extraordinary sound screening in perforated plates. *Phys. Rev. Lett.* **101,** 084302 (2008).
14. Lu, M. *et al.* Extraordinary acoustic transmission through a 1D grating with very narrow apertures. *Phys. Rev. Lett.* **99,** 174301 (2007).
15. Guenneau, S., Movchan, A., Pétursson, G. & Ramakrishna, S. A. Acoustic metamaterials for sound focusing and confinement. *New J. Phys.* **9,** 399 (2007).
16. Ao, X. & Chan, C. T. Far-field image magnification for acoustic waves using anisotropic acoustic metamaterials. *Phys. Rev. E* **77,** 025601(R) (2008).
17. Jacob, Z., Alekseyev, L. V. & Narimanov, E. Optical hyperlens: Far-field imaging beyond the diffraction limit. *Opt. Express* **14,** 8247–8256 (2006).
18. Liu, Z., Lee, H., Xiong, Y., Sun, C. & Zhang, X. Far-field optical hyperlens magnifying sub-diffraction-limited objects. *Science* **315,** 1686 (2007).
19. Ikonen, P., Simovski, C. R., Tretyakov, S., Belov, P. & Hao, Y. Magnification of subwavelength field distributions at microwave frequencies using a wire medium slab operating in the canalization regime. *Appl. Phys. Lett.* **91,** 104102 (2007).
20. Shvets, G., Trendafilov, S., Pendry, J. B. & Sarychev, A. Guiding, focusing, and sensing on the subwavelength scale using metallic wire arrays. *Phys. Rev. Lett.* **99,** 053903 (2007).
21. Kawata, S., Ono, A. & Verma, P. Subwavelength colour imaging with a metallic nanolens. *Nature Photon.* **2,** 438–442 (2008).
22. Sukhovich, A., Jing, L. & Page, J. H. Negative refraction and focusing of ultrasound in two-dimensional phononic crystals. *Phys. Rev. B* **77,** 014301 (2008).
23. Sukhovich, A. *et al.* Experimental and theoretical evidence for subwavelength imaging in phononic crystals. *Phys. Rev. Lett.* **102,** 154301 (2009).
24. He, Z., Cai, F., Ding, Y. & Liu, Z. Subwavelength imaging of acoustic waves by a canalization mechanism in a two-dimensional phononic crystal. *Appl. Phys. Lett.* **93,** 233503 (2008).
25. Cervera, F. *et al.* Refractive acoustic devices for airborne sound. *Phys. Rev. Lett.* **88,** 023902 (2002).
26. Yang, S. *et al.* Focusing of sound in a 3D phononic crystal. *Phys. Rev. Lett.* **93,** 024301 (2004).
27. Ke, M. *et al.* Flat superlens by using negative refraction in two-dimensional phononic crystals. *Solid State Commun.* **142,** 177–180 (2007).
28. Zhang, S., Yin, L. & Fang, N. Focusing ultrasound with an acoustic metamaterial network. *Phys. Rev. Lett.* **102,** 194301 (2009).
29. Yang, Z., Mei, J., Yang, M., Chan, N. H. & Sheng, P. Membrane-type acoustic metamaterial with negative dynamic mass. *Phys. Rev. Lett.* **101,** 204301 (2008).
30. Smith, D. R. & Schurig, D. Electromagnetic wave propagation in media with indefinite permittivity and permeability tensors. *Phys. Rev. Lett.* **90,** 077405 (2003).
31. Torrent, D. & Sánchez-Dehesa, J. Anisotropic mass density by two-dimensional acoustic metamaterials. *New J. Phys.* **10,** 023004 (2008).
32. Kafesaki, M. & Economou, E. N. Multiple-scattering theory for three-dimensional periodic acoustic composites. *Phys. Rev. B* **60,** 11993 (1999).

Acknowledgements

We acknowledge support from the Office of Naval Research (grant number N00014-07-1-0626). L.F. acknowledges a fellowship from the National Science Foundation Graduate Fellowship Program.

Author contributions

J.L. developed the device concept and design. L.F. and J.L. fabricated the device. L.F. and X.Y. constructed the experimental set-up. J.L. and L.F. conducted the theoretical simulations and experiments. X.Z., G.B. and J.L. guided the theoretical and experimental investigations. J.L., L.F., G.B. and X.Z. analysed data and wrote the manuscript.

Additional information

Supplementary information accompanies this paper on www.nature.com/naturematerials. Reprints and permissions information is available online at http://npg.nature.com/reprintsandpermissions. Correspondence and requests for materials should be addressed to X.Z.